Advanced Vehicle Control – Edelmann, Plöchl & Pfeffer (Eds)
© 2017 Taylor & Francis Group, London, ISBN 978-1-138-02992-7

Handling and stability control for an in-wheel-motor-driven electric vehicle

Yue Shi, Hui Lu & Fan Yu
School of Mechanical Engineering, Shanghai Jiao Tong University, Shanghai, P.R. China

ABSTRACT: This work is motivated to enhance the handling and stability performance of an in-wheel-motor-driven electric vehicle (EV). The EV prototype has been developed, and the vehicle parameters have been obtained through practical measurements and road tests. A corresponding multi-body dynamics model of the prototype has been built by using SolidWorks and Adams/Car. An Extended Kalman Filter (EKF) is utilized to estimate the vehicle motion states via a simplified full vehicle model with an empirical tire simulation model which has been verified with the experimental data obtained from CarSim Tire Tester. A fractional order PID (FO-PID) controller is designed for the handling and stability requirements of the EV. Simulations in some typical cases have been carried out, and the results show the effectiveness of the proposed control strategy.

1 INTRODUCTION

From 2010 to 2013, an average of 1.25 million people are killed by road traffic accidents every year, let alone much more injuries, which results in a growing interest in modification of vehicle structure and development of vehicle active safety technologies (WHO, 2015). Electric vehicle (EV) with their wheels independently driven by in-wheel motors is considered as one of the promising structures for future vehicles (Sakai, S. et al. 1999).

In this study, a handling stability control strategy is proposed, as shown in Figure 1. An EV prototype equipped with 4 in-wheel motors is developed by Shanghai Jiao Tong University. A multi-body dynamics model of the prototype is then built accordingly by using SolidWorks and Adams/Car, and serves as the control plant. An 8-DOF vehicle model with a nonlinear tire simulation model is established for calculating vehicle motions. An Extended Kalman Filter (EKF) is utilized to online estimate tire load distribution. A Fractional Order PID (FO-PID) controller is designed to trace the desired yaw motion based on a 2-DOF single-track vehicle model.

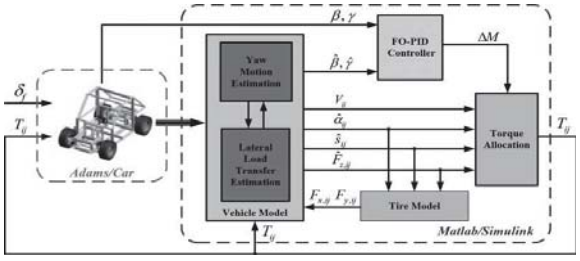

Figure 1. Overall scheme of control strategy.

2 EV PROTOTYPE AND VIRTUAL PROTOTYPING

2.1 *Development of EV prototype*

An EV prototype is developed by Institute of Automotive Engineering, Shanghai Jiao Tong University, as shown in Figure 2. A pair of Li-Ion battery packages, which are consisted of 64 cells, providing about 120V totally, are equipped to power the 4 in-wheel motors each of which can independently generate driving/braking toque to the corresponding wheel. The steering system is modified with an angular sensor mounted on the steering column to measure the steering wheel angle input by driver. The vehicle motion information is measured by an INS/GPS RT3002. The motor driving algorithm is implemented and running online with the utilization of AD5435, a real-time simulation machine. An uninterruptable power supply (UPS) is utilized to power the aforementioned devices.

In cooperation with Shanghai Motor Vehicle Inspection Center, the prototype undergoes a series of practical measurements and road tests, as shown in Figure 3. The obtained main vehicle parameters are presented in Table 1.

Figure 2. EV prototype and equipment.

(a) Test bench (b) Slalom test (c) DLC test

Figure 3. Scenarios of test bench measurement and road tests.

Table 1. Vehicle parameters.

Parameters	Values	Parameters	Values
Mass m (kg)	352.6	Yaw Inertia I_x (kg · m^2)	844.6
CG height h (mm)	370.0	Wheel base L (mm)	1916
Front track width B_f (mm)	1424	Rear track width B_r (mm)	1424
Wheel static load $F_{zs,fl}$ (N)	858.8	Wheel static load $F_{zs,fr}$ (N)	858.8
Wheel static load $F_{zs,rl}$ (N)	869.1	Wheel static load $F_{zs,rr}$ (N)	869.1

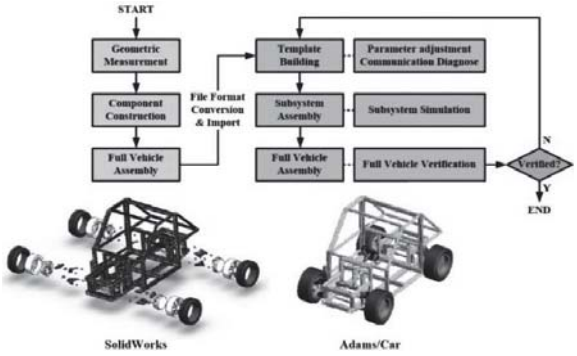

Figure 4. Flowchart of multi-body dynamics modelling.

2.2 *Multi-body dynamics modelling*

Adams is a commercially available virtual prototyping and motion simulation software which can automatically convert a graphically defined model to dynamic equations of motion, and is powerful in simulation and design. However, it is weaker in solid modelling compared to commercial CAD software (Li, Z. & Kota S. 2001). In the presenting study, a multi-body dynamics modelling method using Adams/Car collaborating with SolidWorks is utilized. The flowchart of the modelling procedure is presented in Figure 4.

Based on the geometric information of the EV parts, the physical attributes of the movable elements are respectively built and saved. These individual parts are then assembled by defining their relative position to each other, and the designed degree of freedoms of motion are checked. A symmetric diagnose is carried out to ensure the symmetry of the solid structure. The final version of the full vehicle assembly is locked up and got prepared for the modelling in Adams/Car.

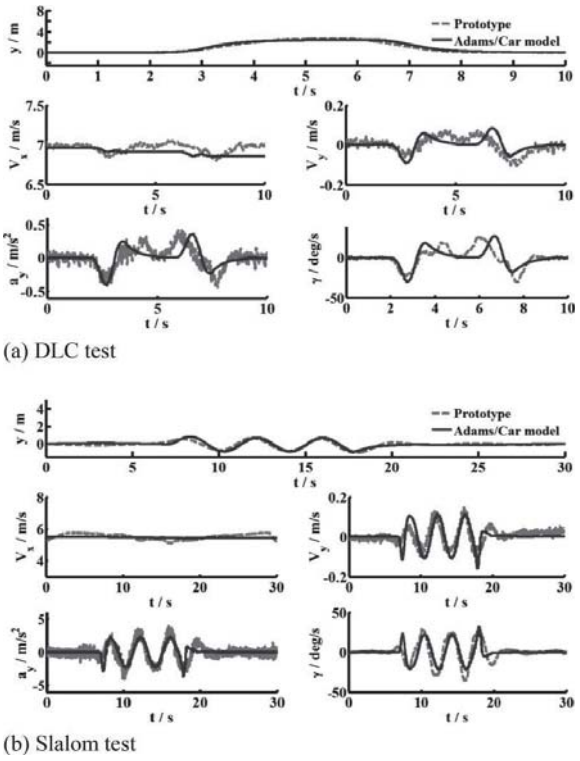

(a) DLC test

(b) Slalom test

Figure 5. Comparison of simulation results with road test data.

Adams/Car provides an access to import a variety of file formats. In this case, Template Building mode is selected, and the SolidWorks files are converted to Parasolid format and imported into Adams/Car. The imported parts are fully created by defining hard points, attachments, feature parameters, mass properties, etc.. The templates are built corresponding to the categories of mechanical subsystems, namely the frame, the front and rear suspensions, the front and rear wheels, the steering system, and the braking system. Communicators are defined for exchanging information among the subsystems. A Joint Torque is built and applied to each in-wheel motor respectively, and defined as State Variable which can be controlled through the algorithms outside Adams/Car. Subsystems are then built based on the corresponding templates, and the multi-body model of the full vehicle is finally assembled.

2.3 *Multi-body dynamics model verification*

After setting the vehicle parameters and iteratively adjusting the characteristics for crucial force elements, the Adams/Car model is established. A series of simulation are carried out, and the results are compared with the experimental data of the road tests. Two typical examples, i.e. the Double Lane Change (DLC) test and the Slalom test, are presented in Figure 5.

In both cases, the virtual prototype is respectively required to trace the same trajectories as those do in the road tests. The driver model embedded in Adams/Car

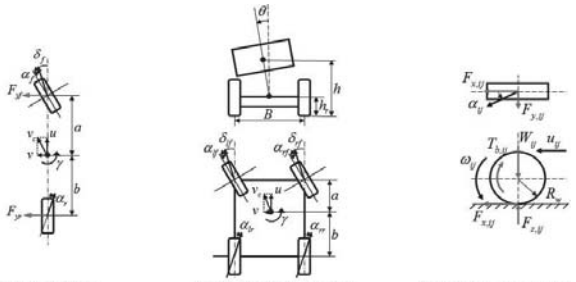

(a) 2-DOF (b) 8-DOF model (c) Wheel model

Figure 6. Vehicle models for controller design.

is adopted. The comparison results of both cases identically indicate that the established Adams/Car model and the physical prototype fit well with each other in characteristics of dynamics responses, which in turn verifies the effectiveness of the established EV model in Adams/Car environment.

3 VEHICLE MODEL AND TIRE MODEL FOR CONTROLLER DESIGN

3.1 *Vehicle model*

To estimate the vehicle states with efficiency and accuracy, some simplified of vehicle models are established, as shown in Figure 6.

3.1.1 *Reference yaw motion*

The reference vehicle yaw motion is calculated by a 2-DOF single-track model, which is shown in Figure 6a, and can be expressed as:

$$\begin{cases} \dot{\beta}_{desired} = \dfrac{1}{mu}\left(F_{y,f} + F_{y,r}\right) - \gamma_{desired} \\ \dot{\gamma}_{desired} = \dfrac{1}{I_z}\left(aF_{y,f} - bF_{y,r}\right) + \Delta M, \end{cases} \tag{1}$$

3.1.2 *Lateral transfer load estimation*

During a harsh cornering, even for the prototype with relatively low CG height and rigid suspensions, the difference between the bilateral tire normal forces is significant, which in turn affects the limit of total tire force of each wheel. Therefore, an 8-DOF vehicle model, as shown in Figure 6b, describing linear and rotational motions about longitudinal and lateral direction, roll motion, and rotational motion of each wheel, is adopted. Considering the tire load distribution as the result of longitudinal and lateral accelerations coupling, the normal force of each wheel can be expressed as

$$\begin{cases} F_{z,fl} = \dfrac{1}{2}m\left(\dfrac{b}{L}g - \dfrac{h}{L}a_x\right) - m\left(\dfrac{b}{L}g - \dfrac{h}{L}a_x\right)\dfrac{h}{Bg}a_y \\ F_{z,fr} = \dfrac{1}{2}m\left(\dfrac{b}{L}g - \dfrac{h}{L}a_x\right) + m\left(\dfrac{b}{L}g - \dfrac{h}{L}a_x\right)\dfrac{h}{Bg}a_y \\ F_{z,rl} = \dfrac{1}{2}m\left(\dfrac{a}{L}g + \dfrac{h}{L}a_x\right) - m\left(\dfrac{a}{L}g + \dfrac{h}{L}a_x\right)\dfrac{h}{Bg}a_y \\ F_{z,rr} = \dfrac{1}{2}m\left(\dfrac{a}{L}g + \dfrac{h}{L}a_x\right) + m\left(\dfrac{a}{L}g + \dfrac{h}{L}a_x\right)\dfrac{h}{Bg}a_y. \end{cases} \tag{2}$$

The state-space representation of the system describe in Eq. (2) is given by

$$\begin{cases} \dot{X}(t) = f\left(X(t)\right) + b_m(t) \\ Z(t) = h\left(X(t)\right) + b_v(t), \end{cases} \tag{3}$$

where the vehicle state vector X is defined as:

$$X = \left[F_{z,fl}\ F_{z,fr}\ F_{z,rl}\ F_{z,rr}\ a_x\ \dot{a}_x\ a_y\ \dot{a}_y\right]^T, \tag{4}$$

and the measurement vector Z is defined as

$$Z = \left[a_x\ a_y\right]^T. \tag{5}$$

The state vector $X(t)$ can be estimated by using the EKF expressed by the following equations:

$$\begin{cases} \hat{X}_{k/k-1} = A_k \hat{X}_{k-1/k-1} \\ P_{k/k-1} = A_k P_{k-1/k-1} A_k^T + Q_k \\ K_k = P_{k/k-1} H_k^T \left(H_k P_{k/k-1} H_k^T + R_k\right)^{-1} \\ \hat{X}_{k/k} = \hat{X}_{k/k-1} + K_k\left(Z_k - H_k \hat{X}_{k/k-1}\right) \\ P_{k/k} = \left(I - K_k H_k\right) P_{k/k-1}, \end{cases} \tag{6}$$

where

$$\begin{cases} A_k = \partial f\left(\hat{X}_{k/k}\right)\big/\partial X \\ H_k = \partial f\left(\hat{X}_{k/k-1}\right)\big/\partial X. \end{cases} \tag{7}$$

3.1.3 *Wheel dynamics*

Considering the vehicle motions within the horizontal plane, the longitudinal and lateral velocities of each wheel are respectively given by

$$\begin{cases} u_{lf} = u - \dfrac{B}{2}\gamma \\ v_{lf} = v + a\gamma, \end{cases} \quad \begin{cases} u_{rf} = u + \dfrac{B}{2}\gamma \\ v_{rf} = v + a\gamma, \end{cases}$$
$$\begin{cases} u_{lr} = u - \dfrac{B}{2}\gamma \\ v_{lr} = v - a\gamma, \end{cases} \quad \begin{cases} u_{rr} = u + \dfrac{B}{2}\gamma \\ v_{rr} = v - a\gamma. \end{cases} \tag{8}$$

Consequently, the sideslip angles can be respectively written as:

$$\alpha_{lf} = \arctan\frac{v_{lf}}{u_{lf}} - \delta_f \quad \alpha_{rf} = \arctan\frac{v_{rf}}{u_{rf}} - \delta_f$$
$$\alpha_{lr} = \arctan\frac{v_{lr}}{u_{lr}} \qquad \alpha_{rr} = \arctan\frac{v_{rr}}{u_{rr}}. \tag{9}$$

The wheel slip ratio of each wheel can be expressed as

$$\begin{cases} s_{ij} = \dfrac{\omega_{ij}R_w - u_{ij}}{\omega_{ij}R_w}, \text{ when } \omega_{ij}R_w \geq u_{ij} \\ s_{ij} = \dfrac{u_{ij} - \omega_{ij}R_w}{u_{ij}}, \text{ when } \omega_{ij}R_w < u_{ij}, \end{cases} \tag{10}$$

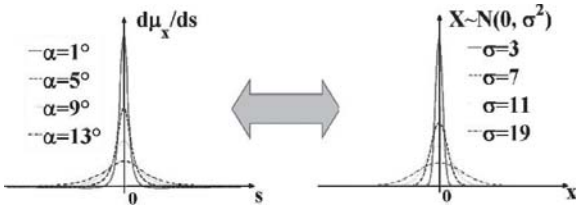

Figure 7. Analogy of curve feature: $d\mu_x/ds$ vs $X \sim N(0, \sigma^2)$.

where the wheel angular velocity ω_{ij} is directly measured by the in-wheel motor. The driving/braking torque is generated by the motor and applied to the wheel, i.e.

$$\begin{cases} J_w\dot{\omega}_{ij} = F_{x,ij}R_w - T_{b,ij}, \text{ when breaking} \\ J_w\dot{\omega}_{ij} = T_{d,ij} - F_{x,ij}R_w, \text{ when accelerating} \end{cases} \tag{11}$$

The estimated tire normal force, wheel slip ratio and sideslip angle will be used as the inputs of the proposed tire simulation model which is to be introduced in Section 3.2, and the lateral force calculated by the tire simulation model will be fed back to actuate the 2-DOF model.

3.2 *Tire model for simulation*

Although many tire models have been thoroughly studied, in this study, a tire simulation model more suitable for the proposed control strategy framework is proposed and described as below.

3.2.1 *Establishment of tire simulation model*

In this work, a tire similar to the ones equipped in the physical prototype is chosen from CarSim database. In order to obtain a suitable mathematical expression, a series of simulation experiments have been carried out to examine the effect of normal force and sideslip angle/wheel slip ratio on tire longitudinal/lateral force. By observing the differential features of the cluster of curves, interesting results shown in Figure 7 have been found out which are presented as below.

From the figure, it can be seen that under a certain normal force, the differential of F_x (or F_y) with respect to s (or α) possesses a similar shape as the normal distribution function (NDF) $X \sim N(0, \sigma^2)$. In addition, when considering combined slip situation, varying α for F_x for example, the curve deflects similarly as the NDF does with respect to different σ. Furthermore, the normal force F_z can be treated as constant around the operation point and eliminated, leaving the the tire-road friction coefficient μ_x (or μ_y) which shares the same shaped of curve as that of F_x (or F_y).

By modifying NDF, the fitting function of $d\mu_x/ds$ (or $d\mu_y/d\alpha$) with respect to s (or α) can be hereby expressed as

$$\begin{cases} \dot{y} = B\left[\dfrac{1}{\sqrt{2\pi}\sigma}\left(e^{-\frac{t^2}{2\sigma^2}} - e^{-\frac{p^2}{2\sigma^2}}\right) + C(t-p)\right] \\ \sigma = p/A, \end{cases} \tag{12}$$

where y represents μ_x (or μ_y), t represents s (or α), p represents s_{px} (or α_{py}) which is the slip ratio (or sideslip angle) corresponding to the maximum value of μ_x (or μ_y).

By integrating Eq. (12), the final format of the proposed tire mathematical expression model can be described as

$$\begin{cases} \mu_x = \int_0^s \dot{\mu}_x dt = A'_x \operatorname{erf}\left(\sqrt{2}\sigma_x s\right) + B'_x s^2 + C'_x s \\ \sigma_x = s_{px}/A_x \\ F_x = \mu_x F_z, \end{cases} \tag{13}$$

$$\begin{cases} \mu_y = \int_0^\alpha \dot{\mu}_y dt = A'_y \operatorname{erf}\left(\sqrt{2}\sigma_y \alpha\right) + B'_y \alpha^2 + C'_y \alpha \\ \sigma_y = \alpha_{py}/A_y \\ F_y = \mu_y F_z, \end{cases} \tag{14}$$

$$\mu_{com} = \sqrt{\mu_x^2 + \mu_y^2} \quad F = \mu_{com} F_z, \tag{15}$$

where

$$A' = \frac{B}{2}, B' = \frac{BC}{2}, C' = -\left(ABC\sigma + Be^{-\frac{A^2}{2}}\Big/\left(\sqrt{2\pi}\sigma\right)\right)$$
$$\operatorname{erf}(x) = \frac{2}{\sqrt{\pi}}\int_0^x e^{-t^2} dt. \tag{16}$$

3.2.2 *Tire model verification*

The proposed tire simulation model for the presented control frame work is then simulated in condition of sweeping F_z, s, and α, and the results are compared with the experimental data of CarSim Tire Tester.

As can be seen in Figure 8a and 8b, the proposed tire simulation model maintains good accuracy throughout the selected region, which in turn suggests that it is feasible to estimate the tire forces by given the information of the operation point (F_z, s, α).

4 CONTROLLER DESIGN AND SIMULATION

4.1 *FO-PID controller design*

As the extension of conventional integer PID controllers, the FO-PID controller with 2 extra tuning parameters, λ and μ, is able to meet more design specifications, and consequently can be more robust to model uncertainty (Chen, Y.Q. et al. 2009). In this study, following the specific instruction by Monje C.A., et al. (2008), an FO-PID controller is designed to trace the desired yaw motion. The transfer function of the controller is defined as:

$$C(s) = PI(s)^{\lambda} \cdot PD(s)^{\mu} = \left(\frac{\lambda_1 s + 1}{s}\right)^{\lambda} \cdot k_c x^{\mu}\left(\frac{\lambda_2 s + 1}{x\lambda_2 s + 1}\right)^{\mu} \tag{17}$$

where $PI(s)^{\lambda}$ is to cancel the phase slope of the plant at desired crossover frequency ω_{cg}, and $PD(s)^{\mu}$ is to

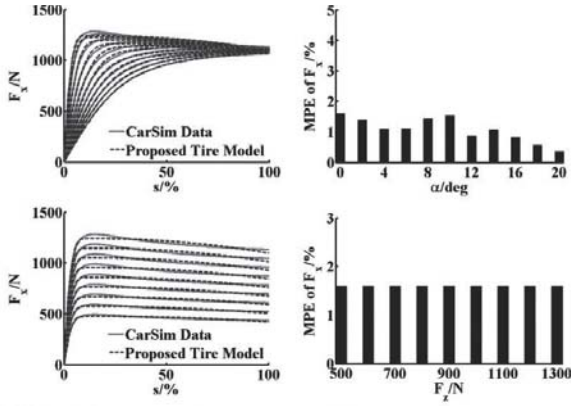

(a) F_x with respect to different α and F_z

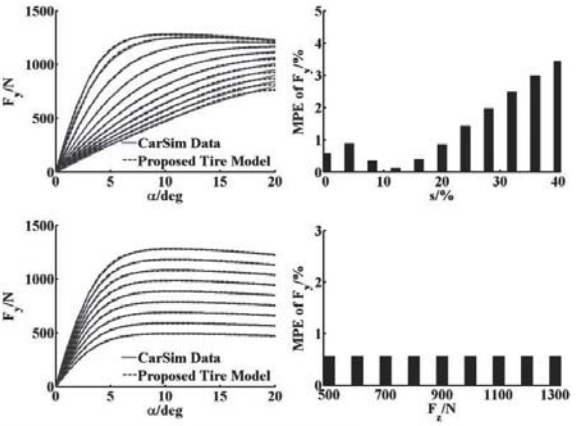

(b) F_y with respect to different s and F_z

Figure 8. Comparison of proposed tire simulation model with CarSim data.

fulfill the design specifications of ω_{cg} and ϕ_m. The design parameters, λ, λ_1, λ_2, μ and x are respectively given as follows.

For $PI(s)^{\lambda}$ controller,

$$\begin{cases} \nu = \dfrac{\phi_u - \phi_{n-1}}{\omega_u - \omega_{n-1}} \dfrac{\text{rad}}{\text{rad/s}} \\ \psi' = \left.\dfrac{\mathrm{d}\psi}{\mathrm{d}\omega}\right|_{\omega=\omega_{cg}} = \lambda \dfrac{\lambda_1}{1+(\lambda_1\omega_{cg})^2} = -\nu \\ \dfrac{\mathrm{d}\psi'}{\mathrm{d}\lambda_1} = \lambda\left[(\lambda_1\omega_{cg})^2 - 1\right] \Big/ \left[1+(\lambda_1\omega_{cg})^2\right]^2 = 0, \end{cases} \tag{18}$$

which gives

$$\lambda_1 = \frac{1}{\omega_{cg}} \qquad \lambda = -2\omega_{cg}\nu. \tag{19}$$

For $PD(s)^{\mu}$ controller,

$$\left[\frac{e^{j(-\pi+\varphi_m)}}{G(j\omega_{cg})PI^{\lambda}(j\omega_{cg})}\right]^{\frac{1}{\mu}} = a + jb$$
$$x = \frac{a-1}{a(a-1)+b^2} \qquad \lambda_2 = \frac{a(a-1)+b^2}{b\omega_{cg}}. \tag{20}$$

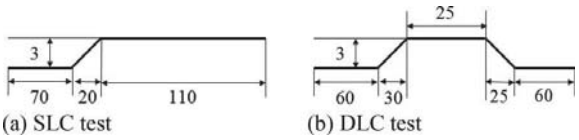

(a) SLC test (b) DLC test

Figure 9. Schematic diagram of simulation trajectory (Unit: m).

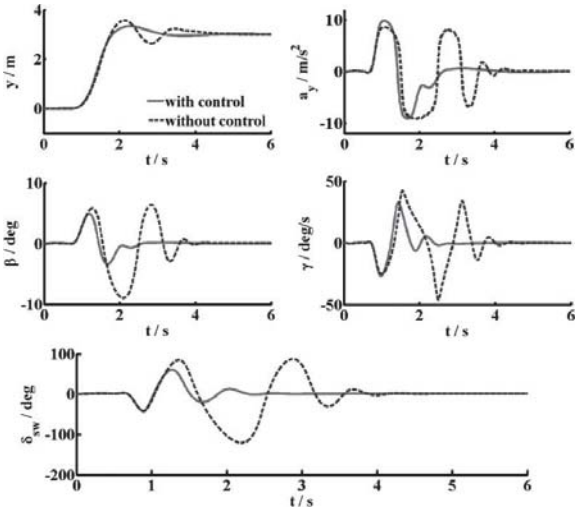

Figure 10. Comparison of performances with/without controller for SLC tests.

where $G(j\omega_{cg})$ represents the transfer function of the reference control plant model which in this case is chosen as a linear bicycle model.

It has been proved that the minimum positive x can ensure the maximum flatness of the phase curve of the compensator (Monje C.A., et al., 2008). Therefore, a very small initial value of μ, e.g. $\mu = 0.01$, is firstly selected, and a corresponding pair of (x, λ_2) can be obtained based on Eq. (20). By slightly increasing μ, the minimum positive x can be obtained and recorded, and the corresponding μ and λ_2 are also recorded as the desired design parameters.

4.2 *Simulation results*

The proposed handling and stability control strategy is implemented on a co-simulation platform established in Adams/Car and Matlab/Simulink. A series of simulations are carried out to examine the effectiveness of the control strategy. The settings of single lane change (SLC) and double lane change (DLC) tests are respectively shown in Figure 9a and 9b.

For the established Adams/Car model, the same driver model embedded in Adams/Car which traces the ideal trajectories via a PID controller is used in both cases with or without help of the proposed controller, respectively. The simulation results are presented below.

Figure 10 shows the motion responses of the virtual prototype and the driver's steering wheel angle input during a single lane change maneuverer. Though the

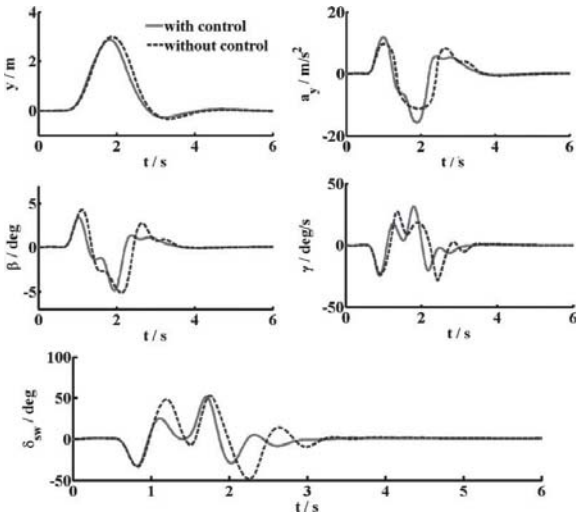

Figure 11. Comparison of performances with/without controller for DLC test.

vehicle is able to fulfill the lane change with or without the assistance of controller, the vehicle with the controller is able to better trace the desired trajectory in responding to driver's steering input. Specifically, the trajectory overshoot is reduced by about 40%, and the stabilization time is reduced by about 1.4 s. On the contrary, without the assistance of the controller, the driver has to roughly sweep the steering wheel in order to maintain the stability of the vehicle and trace the target trajectory. The SLC test shows that the proposed controller is capable of improving the vehicle's dynamics responses and reduce the driving load for the driver.

Similarly, the simulation results of DLC test, shown in Figure 11, also indicate that, with the help of the proposed control strategy, the vehicle handling performance is enhanced, and the driver is able to control the vehicle with less effort. As can be seen in the figure, at the end of each lane change maneuver, the maximum steering wheel angle is reduced from 50° to about 30°. In addition, the stabilization time is reduced by approximately 1 s.

5 CONCLUSIONS

Based on a physical EV prototype, a multi-body dynamics model is built using Adams/Car and SolidWorks, and is verified with road test data. A tire simulation model is designed in order to efficiently and accurately calculate tire forces within the proposed control strategy framework, for which the information of lateral transfer load and vehicle motion variables are estimated by an 8-DOF vehicle model. An FO-PID controller is adopted to improve the stability of the vehicle. Simulation results show that the proposed control strategy is effective to enhance the vehicle performance.

ACKNOWLEDGEMENT

This study is supported by the *National Natural Science Foundation of China* (Grant No. 51375299) and the *Research Program of State Key Laboratory of Mechanical System and Vibration* (Grant No. MSV201505).

REFERENCES

Chen, Y.Q., Petras, I. & Xue, D.Y. Fractional order control-a tutorial [C]. *2009 American control conference. IEEE*, 2009: 1397–1411.

Li Z., Kota S. Virtual prototyping and motion simulation with ADAMS [J]. *Journal of Computing and Information Science in Engineering*, 2001, 1(3): 276–279.

Monje C.A., Vinagre B.M., Feliu V., et al. Tuning and auto-tuning of fractional order controllers for industry applications [J]. *Control engineering practice*, 2008, 16(7): 798–812.

Sakai S., Sado H. & Hori Y. Motion control in an electric vehicle with four independently driven in-wheel motors [C]. *Mechatronics, IEEE/ASME Transactions on*, 1999, 4(1): 9–16.

World Health Organization. *Global status report on road safety 2015* [M]. World Health Organization, 2015.